The Institute of Space and Astronautical Science
Report SP No. 17 March 2003

Assessment of Forebody and Backbody Radiative Heating Rate of Hypervelocity Reentry Capsule

By

Hirotaka OTSU*, Kojiro SUZUKI†, Kazuhisa FUJITA‡, and Takashi ABE‡

(1 February 2003)

Abstract: The thermally and chemically nonequilibrium hypersonic flow around the MUSES-C reentry capsule was analyzed to evaluate the radiative heating environment. The typical reentry speed is 11.6 km/s at the altitude of 64 km. Since the radiative heating strongly depends on the vibrational-electronic temperature distribution, the energy relaxation mechanism for vibrational-electronic energy was clarified by investigating the contribution of each term for energy exchange between translational and vibrational-electronic energy. From this investigation, it was found that the energy relaxation terms related to ions are dominant under such a severe reentry heating environment such as the MUSES-C reentry flight condition. The predicted value for the radiative heat flux at the stagnation point amounts to 1.4 MW/m^2. In the afterbody region, the radiative heat flux is relatively small, and at the base, it is less than 1% of the stagnation point. All around the vehicle surface, the radiative heat flux is much smaller than the convective heat flux. The effect of ablation gas on the radiation was also assessed. It was also found that in the forebody region the effect of the ablative gas on the radiative heating environment for MUSES-C is not so significant but in the afterbody region the effect is relatively large.

1. INTRODUCTION

MUSES-C is the asteroid sample return mission that is scheduled for launch at the beginning of the next century (Kawaguchi et al. 1996). The reentry capsule used for MUSES-C is designed to reenter into the earth atmosphere directly back from the interplanetary orbit in order to reduce the mass and complexity of the system. Since the reentry speed of this capsule is much larger than that of typical reentry from LEO (Lower Earth Orbit), it is expected that the reentry capsule will suffer from much more significant aerodynamic heating environment. According to the preliminary study (Suzuki et al. 1996), the maximum convective heat flux at the stagnation point is supposed to be 10 MW/m^2 at the altitude of 65 km with a velocity of 11.6 km/s, while the radiative heat flux is expected to be 2 MW/m^2. It is well known that, under such a high-speed reentry condition, the radiative heating becomes a more important

* Shizuoka University, Johoku 3-5-1, Hamamatsu, Shizuoka 432–8561, JAPAN.
† University of Tokyo, Hongo 7-3-1, Bunkyo-ku, Tokyo 113–8656, JAPAN.
‡ The Institute of Space and Astronautical Science, Yoshinodai 3-1-1, Sagamihara, Kanagawa 229–8510, JAPAN.

subject for the design of the heat shield system than under a lower speed reentry condition. The radiative heat flux depends on both mass fractions of chemical species and temperatures. Especially, it is very sensitive to the characteristic temperature for the electronic excitation which can be represented by the vibrational-electronic temperature in the two-temperature model (Park 1986). Therefore, in order to analyze the radiative heat flux in detail, we should investigate the mechanism of relaxation process dominating the evolution of the vibrational-electronic temperature.

Additionally, the capsule is designed to use an ablative thermal protection system in order to reduce the aerodynamic heating. It is also well known that the ablation is effective for reducing the convective heating. But the effect of carbon products emitted from the ablative surface on the radiation is yet to be investigated in detail. Especially, in the afterbody region, the ablation products will be distributed not only in the boundary layer but also in the wake region because the density is very low, which means that the flow is chemically frozen, and diffusion is dominant. In that region, temperatures are relatively high, which may produce a strong radiation to the base region of the capsule. So the effect of ablation on the radiation is necessary to investigate for the design of the heat shield system.

The objective of this paper is to examine the thermally and chemically nonequilibrium flow all around the MUSES-C reentry capsule reentering at a superorbital speed and to predict the radiative environment all around the vehicle surface including the effect of surface ablation.

2. AEROTHERMAL MODELS

2.1 Governing equations

The governing equation of the thermally and chemically nonequilibrium flow all around the MUSES-C reentry capsule can be represented by

$$\frac{\partial U}{\partial t} + \frac{\partial F_j}{\partial x_j} = S, \tag{1}$$

where U, F_j, and S are the vector of conserved quantities, flux vector, and the source vector, respectively. In this study, we used an 11-species air model, consisting of N, O, N_2 , O_2, NO, N^+, O^+, $N_2{}^+$, $O_2{}^+$, NO^+, and e^-. Park's two-temperature model (Park 1986) for thermal nonequilibrium is considered. In this model, translational and rotational temperatures are regarded as the common temperature T, while vibrational temperature of each molecule, electronic excitation temperature of each species, and translational temperature of free electron are regarded as the common temperature T_V. The vector of conserved quantities U is as follows;

$$U = (\rho_s, \rho u_j, \rho e, \rho e_V)^t, \tag{2}$$

where ρ_s is the density of each species, u_j is a velocity, e is the total energy of per unit mass, and e_V is the summation of vibrational energy of each molecule, translational energy of free electron, and electronic excitation energy per unit mass. The vibrational energy of each species is calculated using the harmonic oscillator model, while the first two terms of partition function are considered for the electronic excitation energy of each species.

The viscosity of each species is evaluated using the curve fit method (Gupta et al. 1990). The heat conductivity of the translational, vibrational and electron temperature are calculated using an Eucken's relation (Vincenti & Kruger 1965; Cander & MacCormack 1988). The total viscosity and conductivity are calculated using Wilke's semi-empirical mixing rule (Wilke 1950).

As for diffusion, the Schmidt number is assumed to be constant by 0.5. The diffusion coefficients for ions are doubled to take into account the ambipolar diffusion effect.

2.2 Chemical reaction model

We considered 11 species for air consisting of N, O, N_2, O_2, NO, N^+, O^+, N_2^+, O_2^+, NO^+, and e^-, and 6 species for ablation products consisting of C, CO, CN, C_2, C_3, and CO_2. As for rate coefficients for the chemical reactions, Park's reaction set (Park 1990) for air species and Blottner's reaction set (Blottner 1970) for ablation products are considered respectively.

2.3 Thermal nonequilibrium

To take account of thermal nonequilibrium, we considered four terms to describe the relaxation processes in RHS of the vibrational-electronic energy conservation equation. This equation is written in the following form (Gnoffo et al. 1989);

$$\begin{aligned}\frac{\partial}{\partial t}\rho e_V + \frac{\partial}{\partial x_j}\rho e_V u_j &= -P_e\frac{\partial u_j}{\partial x_j} - \frac{\partial}{\partial x_j}\rho e_V v_j + \frac{\partial}{\partial x_j}\left[(\kappa_v + \kappa_e)\frac{\partial T_V}{\partial x_j}\right] \\ &\quad + Q_{T-V} + Q_D + Q_{T-E} + Q_I. \end{aligned} \tag{3}$$

The first term Q_{T-V} is for the relaxation process between translational and vibrational energy and is written in the following form.

$$Q_{T-V} = \sum_{s=molecules} \frac{e^*_{v,s} - e_{v,s}}{\tau_s} \tag{4}$$

where $e_{v,s}$ is the vibrational energy of species s and $e^*_{v,s}$ is the vibrational energy evaluated by T. The relaxation time of each species, τ_s, is calculated using the following expression;

$$\tau_s = \tau_s^{MW} + \tau_s^P, \tag{5}$$

where τ_s^{MW} is the semi-empirical correlation by Millikan and White (Millikan & White 1963). τ_s^P is the correction term suggested by Park (Park 1987) and is effective for $T > 8000K$, which is defined by,

$$\tau_s^P = \left(\bar{N}\bar{c}_s\sigma\right)^{-1}, \tag{6}$$

where $\bar{c}_s$, $\bar{N}$, and σ are the acoustic speed of species s, total number density of heavy particles (Greendyke et al. 1992), and the cross section of vibrational excitation, respectively. For the cross section, we used the curve fit value of Park (Park 1986) given by

$$\sigma = 10^{-21}\left(50000/T\right)^2 \quad [m^2]. \tag{7}$$

The second term Q_D is for the process that a certain amount of energy is removed at dissociation or is added at recombination of molecules. The term is written in the following form.

$$Q_D = \sum_{s=molecules} \omega_s \Delta E_s \tag{8}$$

where ω_s is the mass rate of production of species s and ΔE_s is the amount of the energy shown above. ΔE_s is evaluated as 30% of dissociation energy (Park 1990). This method is called "preferential dissociation model".

The third term Q_{T-E} is for the relaxation process between translational energy of heavy particles and electron. This term is written in the following manner.

$$Q_{T-E} = 2\rho_e \frac{3}{2} \bar{R} (T - T_V) \sum_{s \neq e^-} \frac{\nu_s}{M_s}, \tag{9}$$

where ρ_e, $\bar{R}$, ν_s, and M_s are a density of free electron, a gas constant, a collision frequency of species s and a molecular weight of species s respectively. This term is proportional to the difference between T and T_V, and to the number density of free electron.

The last term Q_I is for the process that a specific amount of energy is removed at ionization caused by electron impact ionization reactions. It is written as,

$$Q_I = - \sum_{s=N^+, O^+} \dot{n}_{e,s} I_s, \tag{10}$$

where $\dot{n}_{e,s}$ is the number density of species s produced by electron impact ionization, and I_s is the ionization potential of species s. The ionization potentials of N and O are 14.53 eV and 13.614 eV, respectively.

Under the high-speed reentry condition expected for MUSES-C, the electron impact ionization becomes dominant for ionization process and the number density of free electron increases exponentially by this chemical reaction. Therefore, the effect of the last two terms is expected to have an important role in the energy relaxation process when ionization occurs severely.

2.4 Model for ablation process

In general, the ablation process is a much complicated process. Nevertheless, since the virgin ablator material changes to a graphite-like material after pyrolysis, we assume that the main ablation process is dominated by the carbon surface chemistry. Unfortunately even though a vast literature exists on carbon surface chemistry and a variety of models for its ablation process were proposed (Zhluktov & Abe 1999), there is no common understanding about what are the main processes on the carbon surface and which is the most reliable model. Here, for simplicity, we assume the simple model which takes into account of the oxidation and sublimation processes on the surface.

The ablation process is classified into two parts, oxidation and sublimation on the surface. For oxidation, we considered the following surface reaction;

$$C(S) + O \rightarrow CO \tag{11}$$

where (S) means the solid. For this reaction, the forward rate coefficient k_w is estimated by

$$k_w = \alpha \sqrt{\frac{RT_W}{2\pi M_s}}, \tag{12}$$

where R, T_W, M_s, and α are gas constant, wall temperature, molecular weight for species s, and reaction probability for the surface reaction respectively. The reaction probability is (Park 1976)

$$\alpha = 0.63 \exp(-1160/T_W). \tag{13}$$

Using the above relations, the mass flux leaving the wall becomes (Keenan & Candler 1993)

$$\dot{m}_{oxi,O} = -\rho_O k_w \tag{14}$$

$$\dot{m}_{oxi,CO} = \frac{M_{CO}}{M_O}\rho_O k_w. \tag{15}$$

The mass flux by sublimation is estimated by the following relation (Blottner 1970);

$$\dot{m}_{sub,s} = \frac{\alpha_s \max(0, p_{evap,s} - p_s)}{\sqrt{2\pi R_s T_W}} \tag{16}$$

where $p_{evap,s}$ and p_s are the equilibrium vapor pressure and the partial pressure of species s respectively. In general, the chemical species produced by sublimation on the surface is considered to be C, C_2, and C_3. The equilibrium vapor pressure is a function of the wall temperature and that of C_3 is much larger than that of C and C_2 (Blottner 1970). Therefore, we considered only the sublimation to C_3. The sublimation coefficient α_s for C_3 is set as 0.023. The equilibrium vapor pressure of C_3 is estimated by the following equation (Blottner 1970);

$$p_{evap,s} = 2.821 \times 10^5 A_s T^{n_s} \exp(-E_s/T) \quad [Pa] \tag{17}$$

where

$$A_s = 4.3 \times 10^{15}, \quad n_s = -1.5, \quad E_s = 97597.0 \tag{18}$$

From the above relations, the total mass flux leaving the wall by ablation becomes

$$\dot{m} = \dot{m}_{oxi,O} + \dot{m}_{oxi,CO} + \dot{m}_{sub,C_3}. \tag{19}$$

Blowing of the ablation gas is assumed to occur in only normal direction to the body. Thus, the injection velocity is calculated by the following relation;

$$v_w = \frac{\dot{m}}{\rho_w}, \tag{20}$$

where ρ_w is the total density at the wall.

3. NUMERICAL METHODS

3.1 Numerical Scheme

In this study, a strong shock wave is formed in front of the capsule and strong expansion occurs around the shoulder. Additionally, to simulate the chemical nonequilibrium, we have to solve the large system equations. For these purposes, we selected the Advection Upstream Splitting Method (AUSM) type scheme (Wada & Liou 1994). This type of scheme can capture a stationary discontinuity with no numerical dissipation and is robust enough to calculate the shock waves and expansions. Additionally, this is a flux splitting type scheme, which is preferable to large system equations.

As for the stiffness problem concerning strong dissociation and ionization reactions, we used a diagonal implicit method (Eberhardt & Imlay 1990). In this study, we approximated the characteristic time for the production, or destruction, of species i, τ_i^c in the following form,

$$\frac{1}{\tau_i^c} \approx \beta \times NS \times \left|\frac{w_i}{\rho_i}\right|, \tag{21}$$

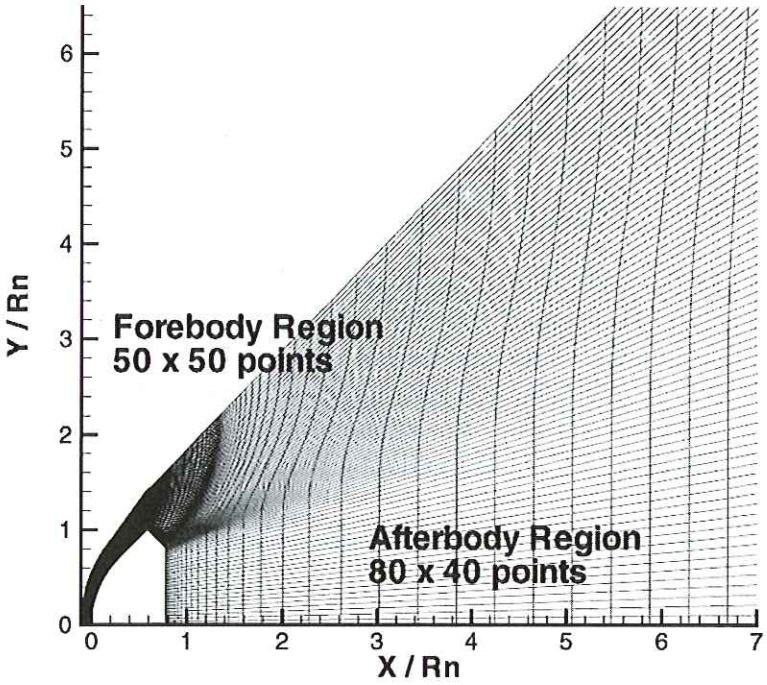

Fig. 1: Computational grid.

where NS is the number of chemical species. From numerical experiments, we found that β is between 1.5 and 0.3. Under the severe calculation conditions, larger value should be used. In this study, 1.5 was used as the initial value and this value can be reduced to 0.3 gradually. A computational grid is composed of two regions, the forebody and the afterbody region. The former contains 50 × 50 grid points and the latter 40 × 80 grid points. The computational grid is shown in Fig. 1.

3.2 Boundary conditions

We consider a typical flight condition in which the reentry speed is 11.6 km/s at the altitude of 64 km. Under this flight condition, both convective and radiative heat flux are expected to be the maximum in the flight path (Suzuki et al. 1996).

As shown in the previous section, the mass loss rate by ablation is strongly dependent on the surface temperature. Especially, the equilibrium vapor pressure $p_{evap,s}$ increases rapidly when the surface temperature becomes greater than 3000 K. Thus, in order to take account of the effect of the wall temperature, we fixed the wall temperature at 3000 K and 3600 K, which corresponds to the oxidation dominant case and the sublimation dominant case respectively. Additionally the ablation is assumed to happen only in the forebody region because the ablation processes are expected to be active only in the region where the aerodynamic heating is significant.

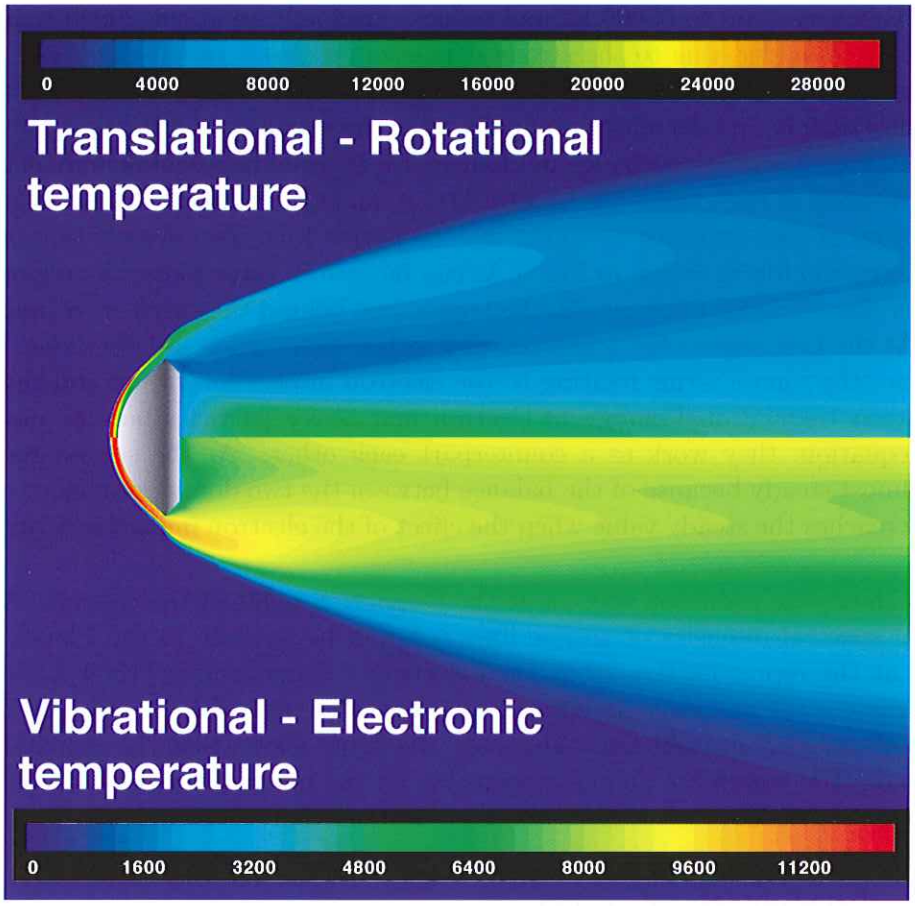

Fig. 2: Distribution of temperatures around the MUSES-C reentry capsule.

3.3 Calculation of radiative heat flux

The radiative heat flux is separately computed by SPRADIAN (version 1.5) (Fujita et al. 1997; Fujita et al. 1998) using the flow field obtained by the flow solver. The emission and absorption coefficients are first calculated at every grid point. Taking account of 3D effects in this system, the radiative heat flux is evaluated by integrating the ray along every line-of-sight. Detailed descriptions of SPRADIAN are presented in the reference (Fujita et al. 1997).

4. RESULTS AND DISCUSSION

4.1 Flow characteristics around the MUSES-C at the trajectory point of peak heating

In this study we focus on the flight condition at the reentry velocity of 11.6 km/s and the altitude of 64 km, when the stagnation heating is expected to become the most intense in the reentry flight path. As for boundary conditions at the body surface, both temperatures are fixed at 3000 K and non-catalytic wall condition is imposed. The MUSES-C reentry capsule is a 45-deg. sphere cone with nose radius of 20 cm, sharpened shoulder, and flat base. Figure 2 shows the distribution of T and T_V around the MUSES-C reentry capsule. Just behind the

bow shock, T increases up to 55000 K, and reduces gradually to about 20000 K in the shock layer. After the shoulder, due to the strong expansion, it drops rapidly to about 4000 K. In the wake region, T is cooled down but increases again due to recompression. T_V in the shock layer is about 11000 K and decreases gradually after the shoulder and in the wake region.

To understand the energy exchange mechanism for thermal non-equilibrium, it is helpful to see the contribution of each term, Q_{T-V}, Q_D, Q_{T-E}, and Q_I, in Eq.(3) for e_V. Figure 3 shows the contribution of each term for e_V along the stagnation line. The distribution of T and T_V along the stagnation line is shown in Fig. 4 As can be seen in these plots, the region inside the shock layer is classified into two regimes; the regime just behind the shock wave and the regime after that. At the first regime the terms relating to the dissociation are dominant. But at the second regime, the source terms relating to the electron impact ionization and the relaxation process between translational energy of electron and heavy particles become dominant. In the energy equation, they work as a counterpart each other. At the second regime, T_V is kept to be almost steady because of the balance between the two dominant counter terms. The temperature reaches the steady value when the effect of the electron impact ionization becomes dominant.

Figure 5 shows the radiation spectra at the stagnation point of the capsule. At the stagnation point, spectral intensity of atomic lines is found to be close to the Planck's radiation distribution at the representative vibrational-electronic temperature (11000 K) in the shock layer. Contribution of molecular band spectra, especially that of $N_2{}^+$ and NO, is relatively large due to chemical nonequilibrium. However, the figure shows that the atomic line spectra in the UV and VUV region are mainly responsible for the net radiative heating of the reentry vehicle (Fujita et al. 1998).

4.2 Effect of computational region

Radiative heat flux at a vehicle surface is calculated by integrating the ray along the line-of-sight to the surface, considering the local emission and absorption. Hence the the computational region must be as large as it does not influence the radiation intensity on the surface. This must be taken care of especially at the base of the capsule. Because the base is exposed to the large dimension of hot wake region. To confirm this, flow calculation was carried out for four computational domains, which are different with the length measured from the base to the edge of the computational region; L_{be}. In this study, the values of L_{be} normalized by the nose radius were employed such as 5, 10, 20, and 30. Figure 6 shows the radiative heat flux at the shoulder and base of the capsule with different L_{be}. The radiative heat flux is normalized by the corresponding values with L_{be}=30. This shows that the radiative heat flux at the base is weakly dependent on L_{be}. The radiative heat flux at the base for L_{be}=5 is less than 95% of that for L_{be}=30. But the radiative heat flux at the shoulder is not quite sensitive to L_{be}. The reason is that T_V close to the shoulder is much higher than in the wake region. Therefore, this region is dominant to the radiative heat flux at the shoulder.

In order to reduce the computational cost, we allowed 5% error for the calculation of the radiative heat flux at the base. So we set L_{be} equal to 10 for the results in the following section.

4.3 Radiative heat flux distribution all around the body

Figure 7 shows distributions of convective and radiative heat flux along the body surface. The convective heat flux at the stagnation point is comparable to the value presented on the Ref.

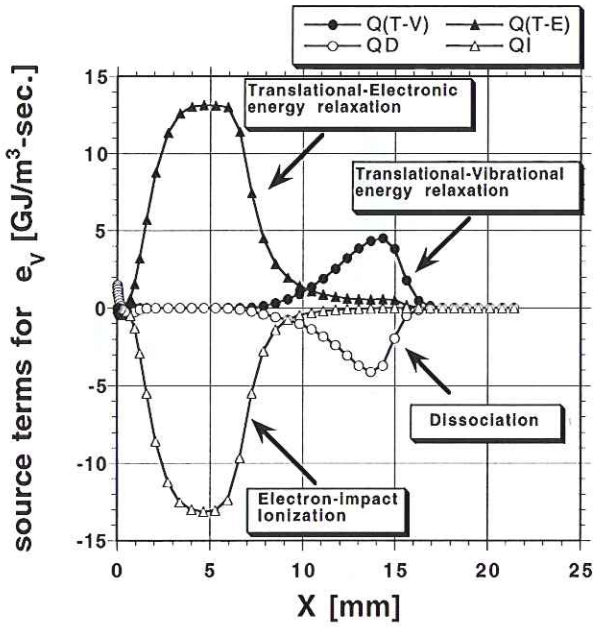

Fig. 3: Contribution of each term e_V along the stagnation line.

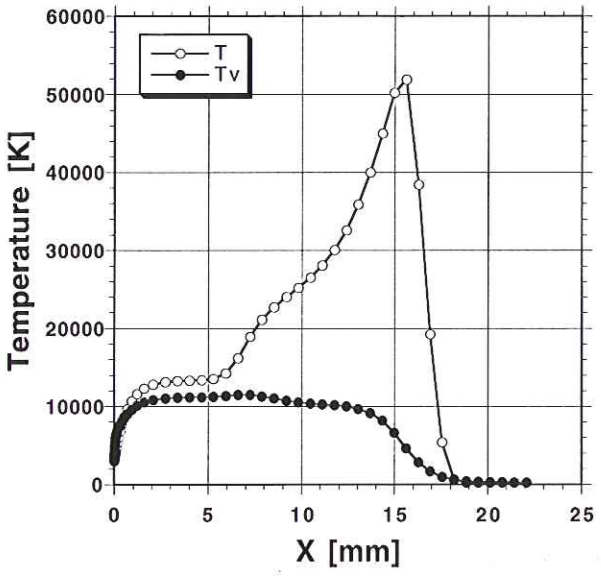

Fig. 4: Distribution of T and T_V along the stagnation line.

(Suzuki et al. 1996). In general, the radiative heat flux decreases gradually along the body surface from the stagnation point to the base of the capsule. In the forebody region, radiative heat flux is smaller than convective heat flux. The radiative heat flux at the stagnation point amounts to 1.4 MW/m^2, which is 30% smaller than the conventionally predicted value 2.0 MW/m^2.

Since both T and T_V decrease after the shoulder, the radiative heat flux also drops rapidly. In the afterbody region, the radiative heat flux is smaller than the convective heat flux, while

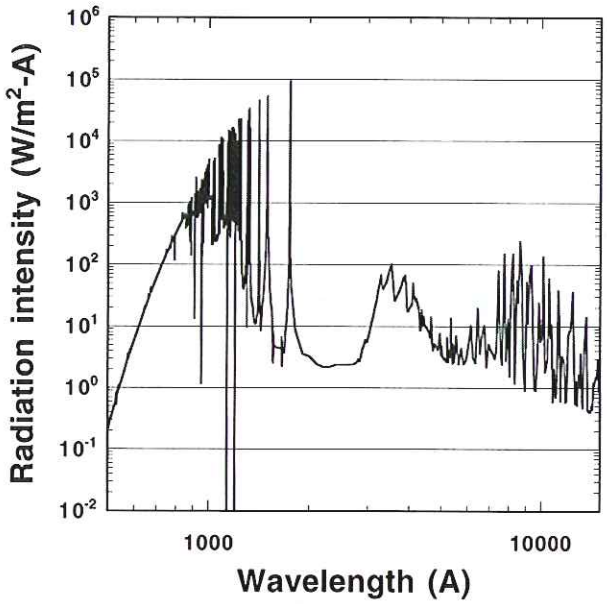

Fig. 5: Radiation spectra from air species at the stagnation point.

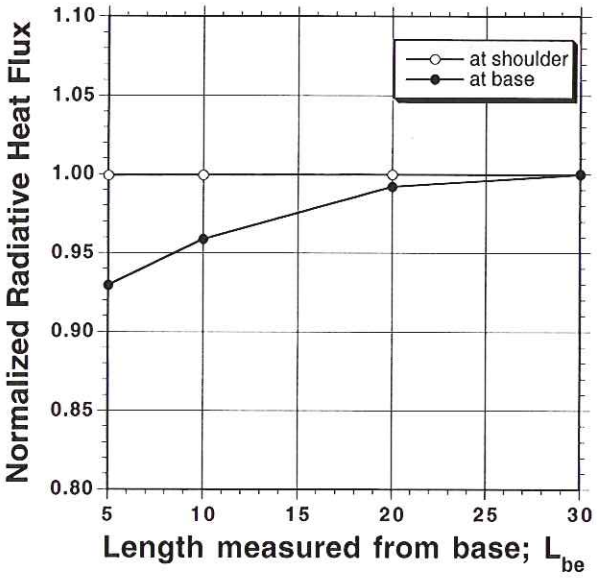

Fig. 6: Effect of computational domain on the radiative heat flux.

the difference between convective and radiative heat flux is relatively small and both convective and radiative heat flux are much smaller than those in the forebody region. At the base, the radiative heat flux is almost constant and the value is less than 1% of the stagnation point.

4.4 Effect of ablative gas on radiative heat flux

The radiation spectra from each ablation product at the stagnation point is shown in Fig. 8. From this figure, we can see that the main source of the radiative heat flux is the atomic carbon

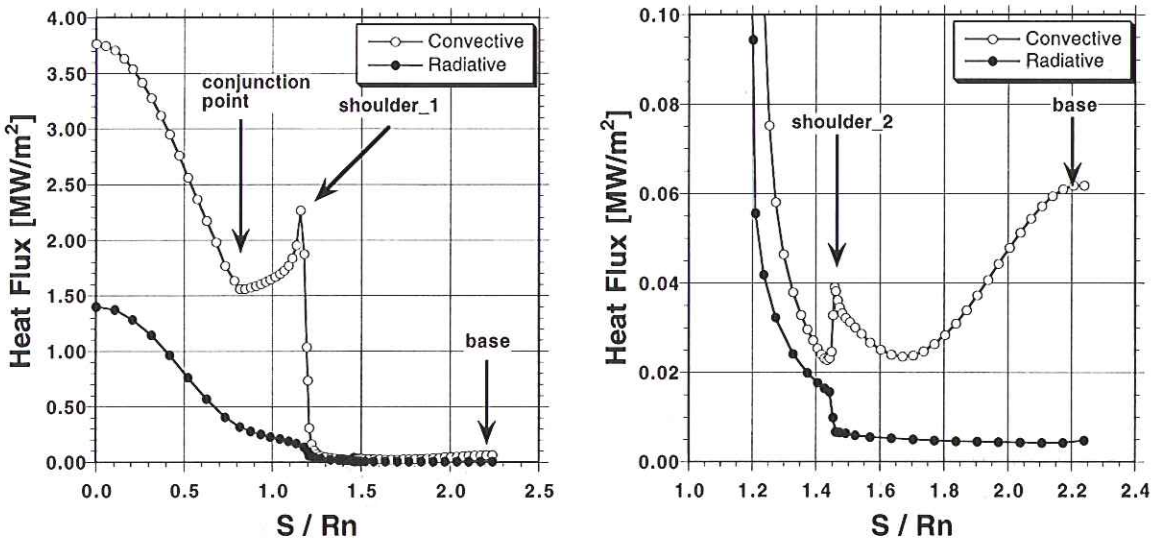

(a) all around the body (b) base region

Fig. 7: Distribution of convective and radiative heat flux around the body surface.

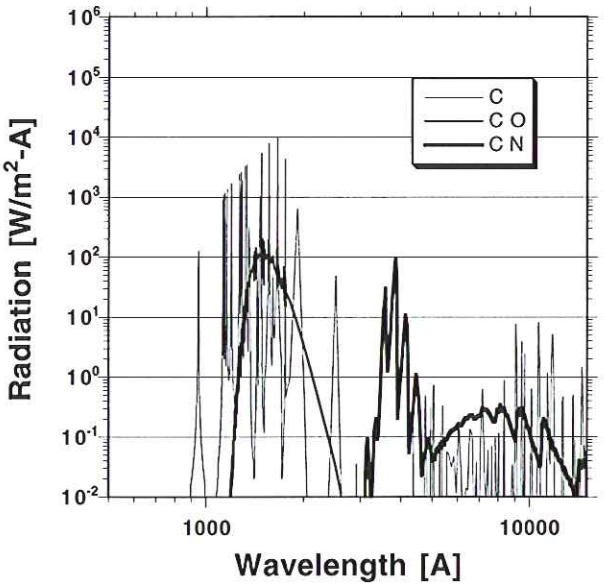

Fig. 8: Radiation spectra from ablation products at the stagnation point.

component in the shock layer. This is because the atomic carbon component is distributed enough outside the boundary layer, where T_V amounts up to about 10000 K, which produces the strong radiation. This means that the radiative heat flux strongly depends on the distribution of the atomic carbon component in the shock lager.

The distribution of the radiative heat flux around the body surface is shown in Fig. 9. The effect of ablation is significant in the forebody region. Around the stagnation point, the

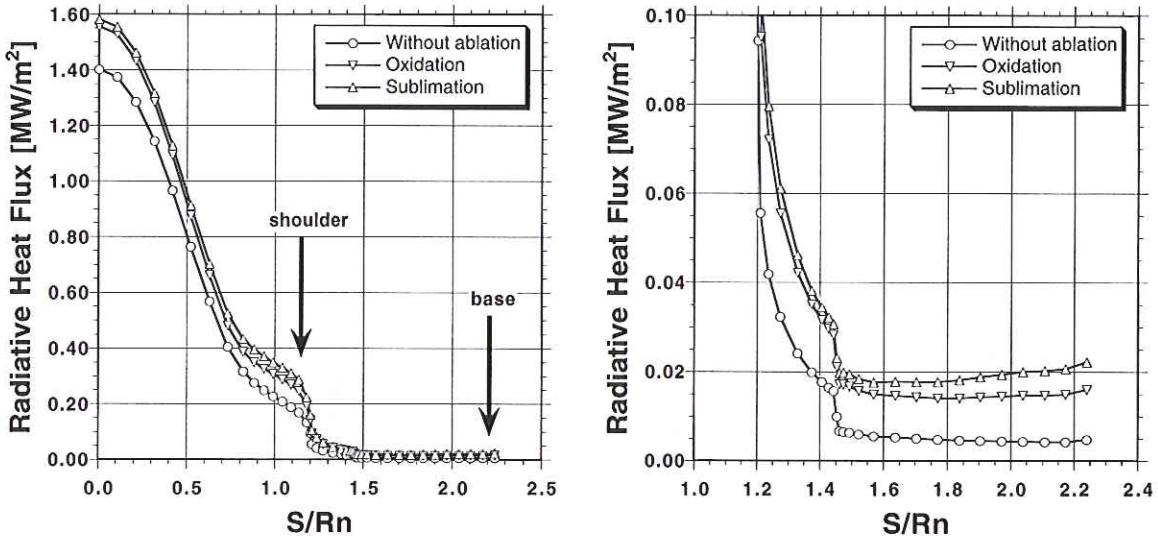

(a) all around the body (b) base region

Fig. 9: Distribution of radiative heat flux around the body surface.

radiation is 10% larger than that of non-ablative surface case. But the difference between oxidation and sublimation dominant case is very small.

The radiative heat flux in the base region is about 1% of that at the stagnation point and is relatively small. But it increases significantly with an amount of ablation gas. This means that, especially at high aerodynamic heating condition, the effect of ablation should be included for estimating the radiative heating.

5. CONCLUSION

In the present study, we analyzed the aerothermodynamic flight environment for the MUSES-C reentry capsule which reenters at a superorbital speed, especially focusing on the radiative heating environment. Since the radiative heating strongly depends on the vibrational-electronic temperature distribution, the energy relaxation mechanism for vibrational-electronic energy was clarified by investigating the contribution of each term for energy exchange mechanisms between translational and vibrational-electronic energy. From this investigation, it was found that the energy relaxation terms related to electrons are dominant under such a severe reentry heating environment such as the MUSES-C reentry flight condition.

The predicted value for the radiative heat flux at the stagnation point amounts to 1.4 MW/m^2, which is smaller than the conventionally predicted value 2.0 MW/m^2. In the afterbody region, the radiative heat flux is relatively small, and at the base, it is less than 1% of the stagnation point. All around the vehicle surface, the radiative heat flux is much smaller than the convective heat flux.

Additionally, the effect of the surface ablation gas on the radiative heat flux was also investigated. The effect of the ablative gas on the radiative heat flux was found not to be so significant. In the forebody region, the increase of the radiative heat flux by the ablative gas was at most 10%. But in the afterbody region, the effect is relatively large.

REFERENCES

Kawaguchi, J., Fujiwara, A., and Sawai, S., "Sample and Return Mission from Asteroid Nereus via Solar Electric Propulsion," *Acta Astronautica*, Vol. 38, No. 2, 1996, pp. 87–101.

Suzuki, K., Kubota, H., Fujita, K., and Abe, T., "Numerical Analysis of Aerodynamic Heating on MUSES–C Reentry Capsule," ISTS 96-d-25, 20th International Symposium on Space Technology and Science, Gifu, Japan, May, 1996.

Park, C., "Assessment of Two-Temperature Kinetic Model for Dissociating and Weakly Ionizing Nitrogen," AIAA Paper, AIAA 86–1347, June, 1986.

Gupta, R. N., Yos, J. M., Thompson, R. A., and Lee, Kam-Pui, "A Review of Reaction Rates and Thermodynamic and Transport Properties for an 11-Species Air Model for Chemical and Thermal Nonequilibrium Calculations to 30,000 K," NASA RP–1232, 1990.

Vincenti, W. G. and C. H. Kruger Jr., *Introduction to Physical Gas Dynamics,* Krieger Publishing Company, Florida, 1965, p. 21.

Candler, G. V. and MacCormack, R. W., "The Computation of Hypersonic Ionized Flows in Chemical and Thermal Nonequilibrium," AIAA Paper, AIAA 88–0511, January, 1988.

Wilke, C. R., "A Viscosity Equation for Gas Mixtures," *Journal of Chem. Phys.,* Vol. 18, No. 4, Apr. 1950, p. 517.

Park, C., *Nonequilibrium Hypersonic Aerothermodynamics,* John Wiley & Sons, Inc., 1990.

Gnoffo, P. A., Gupta, R. N., and Shinn, J. L., "Conservation Equations and Physical Models for Hypersonic Air Flows in Thermal and Chemical Nonequilibrium," NASA TP–2867, 1989.

Millikan, R. C. and White, D. R., "Systematics of Vibrational Relaxation," *Journal of Chem. Phys.,* Vol. 39, No. 12, Dec. 1963, pp. 3209–3213.

Greendyke, R. B., Gnoffo, P. A., and Lawrence, R. W., "Calculated Electron Number Density profiles for the Aeroassist Flight Experiment," *Journal of Spacecraft and Rockets,* Vol. 29, No. 5, 1992.

Park, C., "Assessment of Two-Temperature Kinetic Model for Ionizing Air," AIAA Paper, AIAA 87–1574, June, 1987.

Wada, Y. and Liou, M.-S. "A Flux Splitting Scheme with High-Resolution and Robustness for Discontinuities," AIAA Paper, AIAA 94–0083, January, 1994.

Eberhardt, S. and Imlay, S. "A Diagonal Implicit Scheme for Computing Flows with Finite-Rate Chemistry" AIAA Paper, AIAA 90–1577, June, 1990.

Fujita, K., Abe, T., and Suzuki, K. "Air Radiation Analysis of a Superorbital Reentry Vehicle," AIAA Paper, AIAA 97–2561, June, 1997.

Fujita, K., Abe, T., and Suzuki, K. "UV Radiation Impact on Heating Rate of Super-orbital Reentry Vehicle," ISTS-98-d-39P, 21st ISTS, Omiya, Japan, May, 1998.

Keenan, J. A., and Candler, G. V., "Simulation of Ablation in Earth Atmospheric Entry," AIAA Paper, AIAA 93–2789, July, 1993.

Blottner, F. G. "Prediction of Electron Density in the Boundary Layer on Entry Vehicles with Ablation," NASA SP–252, 1970, pp. 219–240.

Park, C., "Effects of Atomic Oxygen on Graphite Ablation," *AIAA Journal,* Vol. 14, No. 11, 1976, pp. 1640–1642.

Zhluktov, S.V., and Abe, T., "Viscous Shock-Layer Simulation of Airflow past Ablating Blunt Body with Carbon Surface," *Journal of Thermophysics and Heat Transfer,* Vol. 13, No. 1, pp. 50–59, 1999.